IEEE Access
Multidisciplinary | Rapid Review | Open Access Journal

Received August 17, 2020, accepted August 24, 2020, date of publication August 28, 2020, date of current version September 10, 2020.

Digital Object Identifier 10.1109/ACCESS.2020.3020282

16-Port Non-Planar MIMO Antenna System With Near-Zero-Index (NZI) Metamaterial Decoupling Structure for 5G Applications

TAYYAB SHABBIR[1], MOHAMMAD TARIQUL ISLAM[1], (Senior Member, IEEE), SAMIR SALEM AL-BAWRI[2], (Member, IEEE), RABAH W. ALDHAHERI[3], (Member, IEEE), KHALID HAMED ALHARBI[3], ABDULAH JEZA ALJOHANI[3], (Member, IEEE), AND RASHID SALEEM[4]

[1]Department of Electrical, Electronic and Systems Engineering, Faculty of Engineering and Built Environment, Universiti Kebangsaan Malaysia, Bangi 43600, Malaysia
[2]Institut Perubahan Iklim, Universiti Kebangsaan Malaysia, Bangi 43600, Malaysia
[3]Department of Electrical and Computer Engineering, King Abdulaziz University, Jeddah 21589, Saudi Arabia
[4]Department of Telecommunication Engineering, University of Engineering and Technology, Taxila 47050, Pakistan

Corresponding authors: Tayyab Shabbir (tayyab.shabbir@ukm.edu.my), Mohammad Tariqul Islam (tariqul@ukm.edu.my), and Rabah W. Aldhaheri (raldhaheri@kau.edu.sa)

This work was supported by the Universiti Kebangsaan Malaysia Research Grant under grant code MI-2019-015. This work also supported by the Deanship of Scientific Research (DSR) at King Abdulaziz University, Jeddah funded this project under grant No. (RG-2-135-41). The authors, therefore, acknowledge with thanks to DSR technical and financial support.

ABSTRACT In this article, a low-cost 16-port non-planar Multiple-Input-Multiple Output (MIMO) antenna system is proposed for future 5G applications. The non-planar MIMO antenna system is established around a 3D-octagonal-shape polystyrene block. The MIMO elements are arranged on the eight-sides of octagonal-shape block, whereas bottom and top faces of polystyrene block are left void. The single antenna element comprises of slotted microstrip patch with a stepped chamfered feed line and defected ground plane. Each MIMO element is designed on FR-4 substrate with a size of 22 mm $\times$ 20 mm, to cover the frequency band of 3.35 GHz to 3.65 GHz for the fifth-generation (5G) applications. The isolation between array elements is improved by using a meander-lines based near-zero-index epsilon-negative (NZI-ENG) metamaterial decoupling structure. The array elements are placed on the top-layer, whereas common connected ground plane and decoupling structure is placed on the bottom-layer. The metamaterial-based decoupling structure offers an isolation of more than 28 dB for antenna elements arranged in across and side-by-side configuration. Moreover, simulated and measured MIMO performance parameters i.e. Total Active Reflection Coefficient (TARC) < -18 dB, Envelop correlation coefficient (ECC) < 0.1 and Channel capacity loss (CCL) $<$ 0.3 are in acceptable limits. The proposed non-planar 3D-MIMO antenna system can be employed for indoor localization systems and wireless personal area network applications, where different 5G devices are wirelessly linked to a centralized server. Moreover, a good agreement between simulated and measured results is achieved for the non-planar MIMO antenna system.

INDEX TERMS Antenna, channel capacity loss (CCL), common ground plane, envelope correlation coefficient (ECC), fifth-generation (5G), epsilon negative metamaterial (ENG-MTM), multiple-input-multiple-output (MIMO).

I. INTRODUCTION

The future fifth-generation (5G) communication era will play an important role in the evolution of wireless communication systems [1]. The Multiple-Input-Multiple Output (MIMO) technology integration with 5G communication has the capability to increase the channel capacity, spectral efficiency and transmission rates with minimum delays [2]. Therefore, the microwave research community has put significant efforts to design the 5G-MIMO antenna systems. The integration of multiple MIMO elements in a limited space is a major design challenge in the 5G-MIMO antenna design [3]. In MIMO

The associate editor coordinating the review of this manuscript and approving it for publication was Jinming Wen.

configuration, each radiating array element should be miniaturized, well-matched, and has a low mutual coupling with neighbouring array elements. However, due to space constraints, closely placed antenna elements produce high mutual coupling, which is undesirable and reduced the performance of the MIMO antenna system. Therefore, an effective decoupling structure is required to reduce the mutual coupling between array elements [4], [5]. In the literature, numerous techniques have been investigated to integrate multiple MIMO elements with acceptable isolation between the array elements. These techniques include but are not limited to Frequency Selective Surfaces (FSSs) [6], neutralization lines [7], Defected ground Structures [8], metamaterial isolators [9] and parasitic elements [10]. Among these decoupling techniques, metamaterial-based decoupling structures have been widely used due to their unique electromagnetic characteristics. The metamaterial-based decoupling structures provide high isolation in closely placed array elements.

A mu-negative (MNG) metamaterial structure in [11], is employed to obtain low mutual coupling among monopole antennas at 2.67 GHz frequency band. Furthermore, a correlation coefficient of less than 0.02 and mutual coupling less than -25 dB is realized for the proposed MIMO antenna configuration. A dual-port microstrip patch antenna with a flower-shaped metamaterial structure is proposed in [12]. The flower-shaped metamaterial decoupling structure provides isolation of about 30 dB, TARC < -12 dB and peak gain of 5 dBi for the WiMAX frequency band. In another study, split-ring resonator-based metamaterial decoupling structure is employed to isolate the multi-band MIMO elements. In this work, a correlation coefficient of less than 0.04 is achieved, and mutual coupling never exceeds -20 dB for a two-port array configuration [13]. A microstrip patch antenna array with dual-polarization and metamaterial slabs is proposed in [14]. In this MIMO configuration, split-ring resonators based metamaterial decoupling structure is employed to reduce the mutual coupling between array elements. In [15], mutual coupling reduction between two antenna elements is achieved by employing coupled split-ring resonators for the 5.3 GHz frequency band. The metamaterial-based decoupling is used to achieve an isolation of more than 25 dB between array elements. A wheel-like metamaterial decoupling structure is proposed in [16]. This metamaterial-based decoupling structure provides a peak gain of 4.62 dBi and isolation of 20 dB in $8-12$ GHz frequency band.

In the existing literature, different MIMO designs are reported for non-planar and planar array configurations. A compact 3D non-planar array with two elements is reported in [10]. The MIMO radiating elements are arranged around a square polystyrene block. A parasitic decoupling structure with C-shape slits and vertical-stubs are used to realize isolation of 20 dB within non-planar array configuration. Another non-planar array with four antenna elements is presented in [5]. FSS-based decoupling is employed to isolate the array elements. The mutual coupling between array elements never exceeds -20 dB for 3D non-planar array configuration. A compact miniaturized non-planar array with eight-elements is proposed in [17]. A modified π-shaped parasitic decoupling structure is used to decrease the mutual coupling in the 3D-octagonal arrangement. Moreover, ECC < 0.0025, TARC < -11 dB, CCL < 0.35 and isolation better than 20 dB is attained for proposed non-planar MIMO antenna system. In [18], antenna array with eight radiating elements is reported for non-planar configuration. The isolation enhancement between array elements is achieved by arranging four array elements in a horizontal configuration while remaining four in a vertical configuration. A MIMO antenna system with eight radiating elements for 3.5 GHz smartphone applications is proposed in [2]. A good impedance matching along with ECC < 0.05 is realized for 5G communication. In [19], a dual-band ten-elements MIMO antenna system for 5G terminal applications is proposed. The proposed MIMO configuration provides isolation of more than 12 dB, efficiency is greater than 45% and ECC < 0.15 for 5G communication. A planar MIMO antenna system with twelve-ports is proposed for fifth-generation smartphone applications [20]. This array configuration covers the 3.5 GHz frequency band with the isolation of more than 20 dB between array elements. In another study, 8-port MIMO antenna system with slots and stubs is reported in [21], an isolation level better than 15 dB, efficiency more than 70%, and envelop correlation coefficient below 0.05 realized for metal-rimmed smartphones.

In this paper, a 16-port non-planar MIMO antenna array with NZI-ENG metamaterial decoupling structure is proposed for future 5G applications. The fabricated 16-port MIMO antenna system with a polystyrene block is illustrated in Fig. 1. The MIMO elements in the non-planar configuration are placed on the 3D octagonal-shaped polystyrene block. A meander-lines based near-zero-index epsilon-negative (NZI-ENG) metamaterial decoupling structure is employed to achieve an isolation of more than 30 dB for antennas placed in across and side-by-side arrangement. Moreover, performance parameters of the MIMO antenna system: CCL, TARC and ECC are in acceptable limits. The proposed MIMO antenna system is designed and analyzed by using a full-wave ANSYS High-Frequency Structural Simulator (HFSS®). The proposed high isolated, non-planar MIMO antenna system can be used for the wireless personal area network applications, where different 5G devices are wirelessly linked to a centralized server in a rich scattering environment. Moreover, non-planar MIMO antenna system can be employed for indoor localization systems. Where high accuracy via sophisticated coverage area, higher capacity system, multipath component rejection and less number of reference units are considered as the main features of implementing such type of MIMO antenna system for indoor localization technique due to its capability to cover a 360° mechanism with a distributed 16-port omnidirectional antennas for indoor localization scenario, each element with higher gain up to 6.5 dBi at 3.5 GHz. This paper is structured as follows: in Section II design and analysis of metamaterial is discussed. The 16-port MIMO antenna design

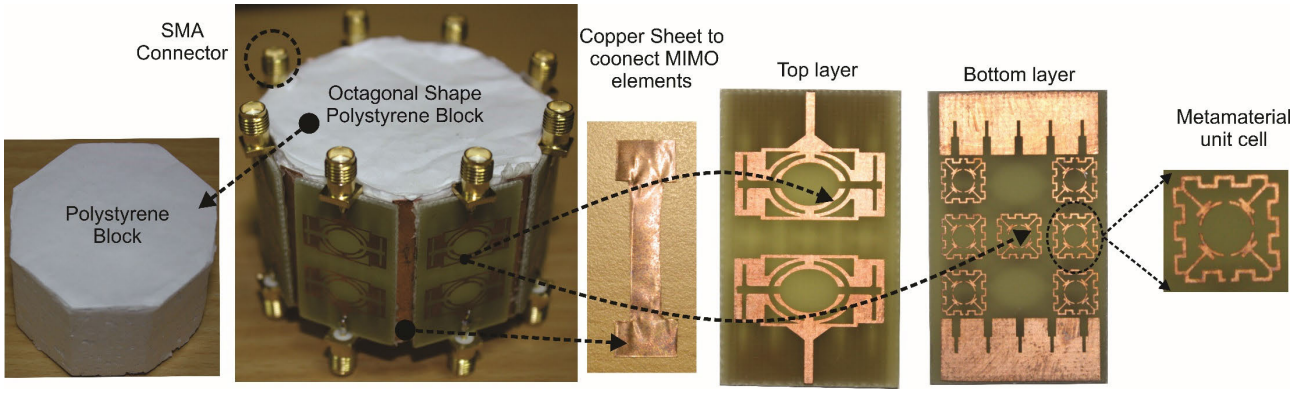

FIGURE 1. Fabricated 16-port non-planar MIMO antenna system.

TABLE 1. Optimized parameters of metamaterial unit element.

Parameters	a,b	r_1, r_2	a_1	a_2	a_3	a_4	a_5
value(mm)	8, 8	8, 2	8.7	2.3	10.5	5.6	15.3
Parameters	a_6	a_7	a_8	a_9	a_{10}	c_1	c_2
Value(mm)	4	8.2	2.90	3.83	10	3.5	3.55

and methodology is described in Section III. The simulated and measured results are described in Section IV, including impedance matching, isolation and far-field radiation characteristics. Finally, Section V concludes the paper.

II. DESIGN AND ANALYSIS OF METAMATERIAL

The metamaterial structure is designed on a low-cost FR-4 substrate (relative permittivity = 4.4 and loss tangent = 0.02), thickness of 1.5 mm and copper cladding of 0.035 mm. Metamaterial simulations are performed in the commercially available full-wave HFSS software. The MTM unit element consists of a meander-lines based square ring attached with T-shape stubs and circular split ring. A 0.3 mm split is introduced on the left side of a meandered square ring. Each corner of the square ring is attached with the T-shape stubs. Finally, a circular ring with four splits at 0°, 90°, 180° and 270° angles is attached at the center of the square ring. The proposed metamaterial design, configuration and analysis setup is illustrated in Fig. 2. Moreover, Table 1 shows the optimized metamaterial unit element parameters. The meander-lines based metamaterial structure is arranged between two wave ports, one along negative and another along the positive z-axis. The proposed metamaterial structure negative characteristics are achieved by placing in perfect magnetic (x-axis) and perfect electric (y-axis) boundaries [22]–[24], as illustrated in Fig. 2b. Furthermore, metamaterial structure physical phenomena is explained by using surface current distribution. Fig. 3 shows the surface current distribution on the metamaterial structure at 3.5 GHz frequency. The high surface current concentration is observed on the three sides of the meandered square ring and T-shape stubs. Whereas, a low surface current distribution is perceived on the splits in the inner circular-ring and left side of meander-lines geometry.

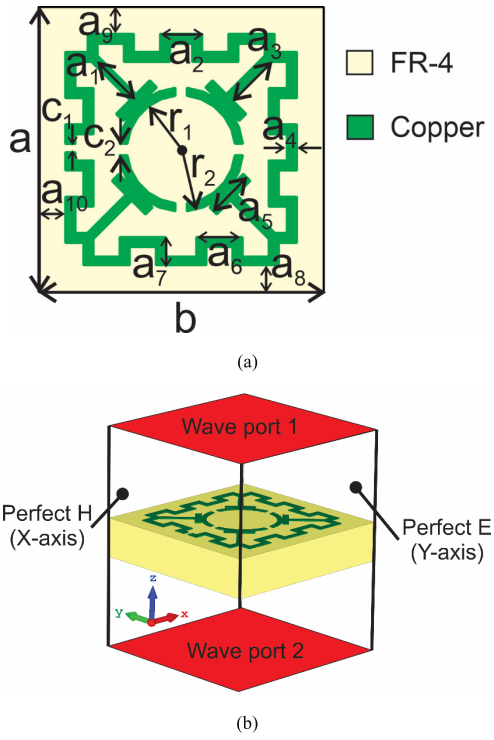

FIGURE 2. Geometry, configuration, and analysis of metamaterial element. (a). Unit element geometry. (b). Analysis setup.

Moreover, surface current flows in the opposite direction in the circular split-ring. This current direction reversal, along with strong surface current distribution on the meandered square ring and T-shape stubs, creates a good stop-band at 3.5 GHz frequency band.

$$S_{11} = \frac{R_{01}\left(1 - e^{i2n\kappa_0 d}\right)}{\left(1 - R_{01}^2 e^{i2n\kappa_0 d}\right)} \quad (1)$$

$$S_{21} = \frac{\left(1 - e^{i2n\kappa_0 d}\right)}{\left(1 - R_{01}^2 e^{i2n\kappa_0 d}\right)} \quad (2)$$

$$R_{01} = \frac{(Z-1)}{(Z+1)} \quad (3)$$

$$\text{Real (z)} \geq 0 \quad (4)$$

$$\text{Imaginary (n)} \geq 0 \quad (5)$$

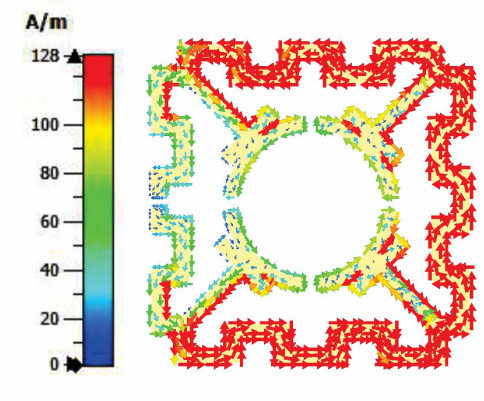

FIGURE 3. Surface current distribution on metamaterial unit cell at 3.5 GHz frequency.

$$z = \pm\sqrt{\frac{(1+S_{11})^2 - S_{21}^2}{(1-S_{11})^2 - S_{21}^2}} \tag{6}$$

$$e^{i2n\kappa_0 d} = \frac{S_{21}}{1 - S_{11}\frac{Z-1}{Z+1}} \tag{7}$$

$$n = \frac{1}{k_0 d}\left\{\left[Im.\left[\ln e^{ink_0 d}\right] + 2m\pi\right] - i\left[Re.\left[\ln e^{ink_0 d}\right]\right]\right\} \tag{8}$$

$$\varepsilon = \frac{n}{z} \tag{9}$$

$$\mu = nz \tag{10}$$

The scattering parameters (reflection and transmission coefficient) of the metamaterial unit element are plotted in Fig. 4. The meander-lines based square split-ring, T- shaped stubs and circular ring creates an effective stop-band at the 3.5 GHz frequency band. The metamaterial structure usually acts like an inductance-capacitance (LC) resonator. The gaps/splits create a capacitive effect, whereas stubs and metallic rings are responsible for the inductive effect. The metamaterial structure resonant characteristics are typically controlled by gaps, stubs and metallic rings [25].

A robust method in [25], [26] is utilized to obtain the effective permittivity, effective permeability and effective refractive index for 2 – 6 GHz frequency band. The S-parameters and metamaterial characteristics are shown in Fig. 4. A good stop-band response is achieved at the 3.5 GHz frequency band. Equations (1) to (10) provided in [25], [26], [38] are employed to extract the effective parameters (permittivity, permeability and refractive index), as shown in Figs. 4b – 4d. For 3.4 – 3.6 GHz frequency band, NZI-ENG metamaterial characteristics are achieved. The metamaterial structure contains negative permittivity, near-zero permeability and negative refractive index in the intended frequency band.

III. SIXTEEN PORT NON-PLANAR MIMO ANTENNA SYSTEM

Initially, a slotted microstrip patch antenna operating in 3.4 to 3.6 GHz frequency band is designed on a low-cost FR-4 substrate. Secondly, 1 × 2 elements MIMO antenna system is designed. The array elements are decoupled by employing

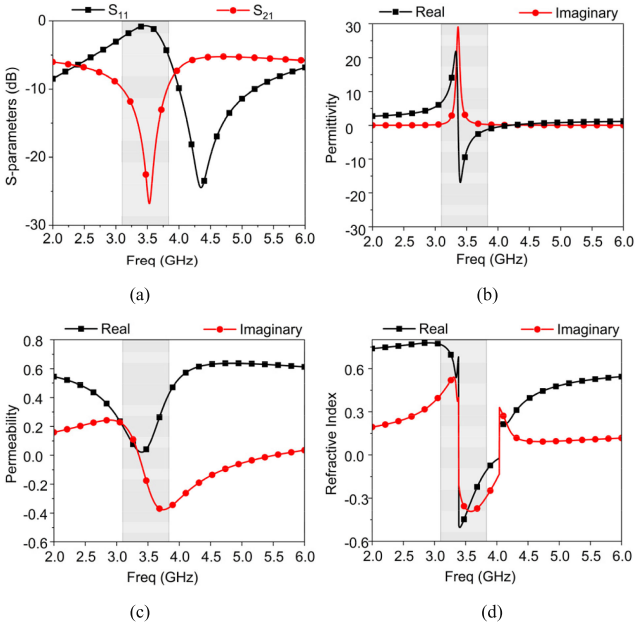

FIGURE 4. Simulated metamaterial effective parameters. (a). S-parameters. (b). Permittivity. (b). Permeability. (d). Refractive index.

a meander lines-based metamaterial decoupling structure on the flip-side of the substrate. Finally, 16-port MIMO antenna system for the non-planar arrangement is designed around an octagonal-shaped polystyrene block with a common connected ground plane for fifth-generation applications.

A. UNIT ELEMENT AND 1 × 2 ARRAY ANALYSIS

The single antenna element with compact dimensions of 20 mm × 22 mm size is designed on 1.5 mm thick FR-4 substrate (dielectric constant = 4.4, loss tangent = 0.02). The single antenna element comprises of a slotted microstrip patch on the top-layer, whereas defected ground structure is placed on the rear-side of the substrate. The radiating patch consists of T-shape slots and pair of circular split-rings, to obtain a good impedance matching in 3.4 to 3.6 GHz frequency band. A stepped chamfered structure is attached to the feed line and radiating patch. This stepped structure acts as an impedance transformer and provides better impedance matching in the desired frequency band. The defected ground plane structure at the bottom-layer also contributes to control the resonance and impedance matching in 3.4 to 3.6 GHz frequency band. Fig. 5 shows the single antenna element geometry and configuration.

The optimized parameters of a single antenna element to achieve resonance at 3.5 GHz frequency band are shown in Table 2. The design methodology of a single antenna element (radiating patch and ground plane) is illustrated in Fig. 6. The different design modifications in the ground plane and radiating patch are shown in Fig. 6. The design amendments effect on the reflection coefficient is observed, to achieve proper impedance matching in 3.4 to 3.6 GHz frequency band. Microstrip patch antenna shown in design-A, provides a resonance at 5 GHz frequency band. A stepped

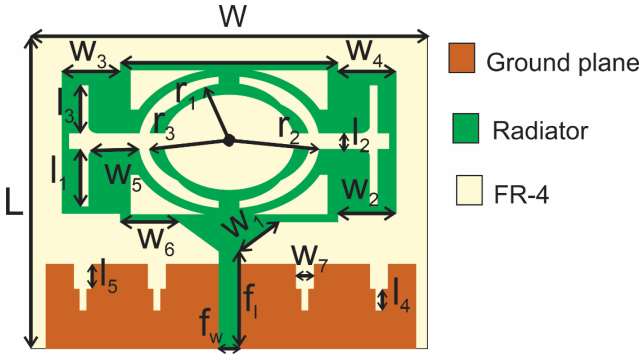

FIGURE 5. Single element antenna geometry and configuration.

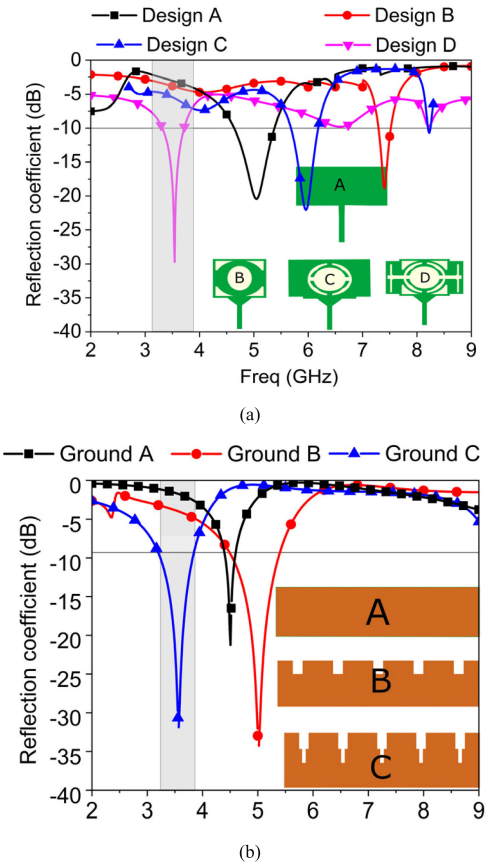

FIGURE 6. Design methodology of single antenna element. (a). Patch shape selection. (b). Ground plane alteration.

structure is introduced and attached with a feed line, as shown in design-B. This stepped structure acts as an impedance transformer. By decreasing the microstrip patch size, resonance is shifted towards a higher frequency band.

The impedance matching at the lower frequency band is achieved by introducing a pair of circular split-ring resonators, and T-shape slots in the main radiator, as illustrated in design- C and D. Finally, a good impedance matching in 3.4 to 3.6 GHz frequency band is attained for the slotted microstrip patch. The ground plane design methodology and shape variation effect on the reflection coefficient is plotted

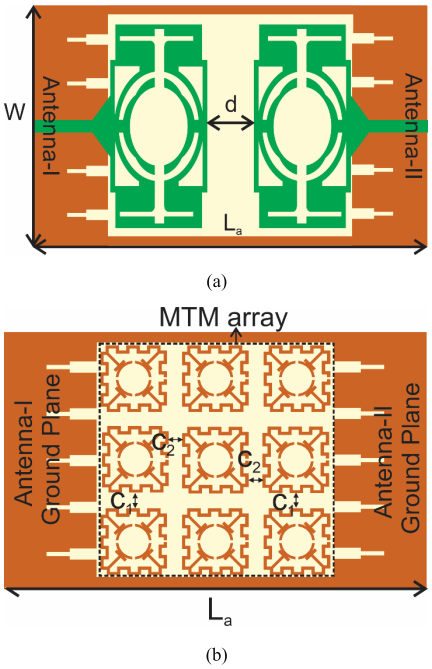

FIGURE 7. 1 × 2 MIMO antenna configuration. (a). MIMO array without decoupling structure. (b). MIMO array with metamaterial-decoupling structure.

TABLE 2. Optimized parameters of a single element and 1 × 2 MIMO array.

Parameters	L	W	f_l	f_w	W_1	W_2	W_3,W_4
value(mm)	20	22	5.4	1.2	2.76	3.24	3.24
Parameters	d	W_5	W_6	W_7	r_1	r_2	r_3
Value(mm)	4.2	2.28	3.25	0.7	3.9	4.9	4.5
Parameters	l_1	l_2	l_3	l_4	l_5	C_1,C_2	L_a
Value (mm)	3.1	0.9	2.8	2	2.3	1.32	36, 4.2

in Fig. 6(b). By decreasing the ground plane height, resonance shifts towards a higher frequency band. The defected ground plane structure at the flip-side of the FR-4 laminate helps to achieve a wide-band resonance at 3.5 GHz frequency.

A 1 × 2 MIMO antenna system with radiating elements and metamaterial decoupling structure is illustrated in Fig. 7. This two-port array arrangement has dimensions of $L_a \times W$. Besides, two antenna elements are placed on the FR-4 substrate with 180° angle and 4.2 mm vertical distance between them, as shown in Fig. 7 (a). The metamaterial-based decoupling structure is employed to enhance the isolation among the array elements. A near-zero-index epsilon-negative (NZI-ENG) metamaterial structure is placed on the bottom-side of the main radiating elements, as shown in Fig. 7(b).

The S-parameters of 1 × 2 MIMO antenna system without a decoupling structure is plotted in Fig. 8(a). In the absence of the metamaterial decoupling structure, high mutual coupling is observed for the dual-port MIMO antenna system. The

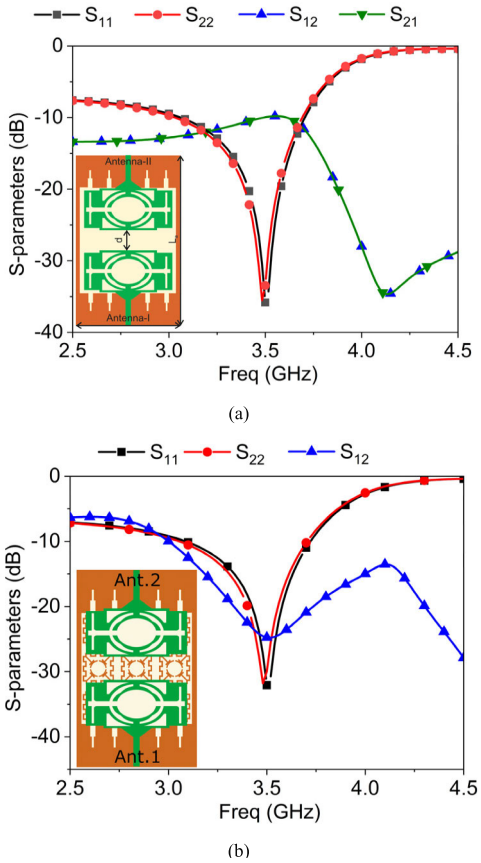

FIGURE 8. 1 × 2 MIMO antenna system S-parameters. (a). Without MTM decoupling structure. (b). With MTM decoupling structure.

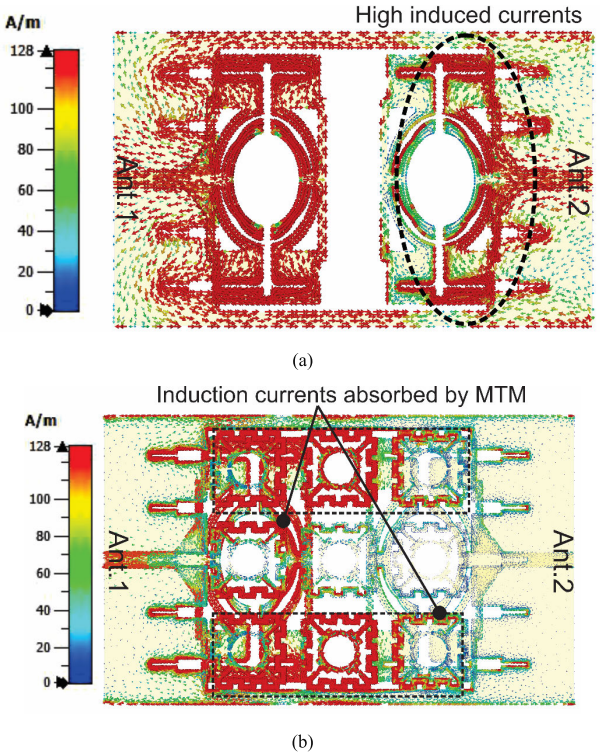

FIGURE 9. 1 × 2 MIMO antenna system surface current distribution. (a). Without MTM decoupling structure. (b). With MTM decoupling structure.

surface distribution is used to show the effectiveness of the metamaterial decoupling structure. High induced currents are observed on antenna 2, without the decoupling structure, which is undesirable, as shown in Fig. 9(a). A metamaterial-based effective decoupling structure is employed for the mutual coupling reduction among MIMO array elements. The S-parameters of the two-element MIMO antenna system with metamaterial decoupling structure is shown in Fig. 8(b). A significant reduction in mutual coupling along with isolation of more than 30 dB is realized with a metamaterial decoupling structure. The surface current distribution in the presence of the decoupling structure is shown in Fig. 9(b). The MTM decoupling structure suppresses the unwanted induced currents on the antenna 2. This suppression of unwanted induced currents helps to improve the isolation between MIMO elements.

B. SIXTEEN PORT 5G MIMO ANTENNA SYSTEM

A 16-port MIMO antenna system is designed to create a strong and reliable communication link in a rich scattering environment. These types of MIMO antenna systems with off devices can be used for the production lines or hospital rooms, where the best reception is required. The array elements are placed on the octagonal-shaped polystyrene block. The polystyrene block has a dielectric constant of 2.6; each face height is 36 mm and width is 23 mm. The array elements are arranged in a 3D octagonal-shape arrangement. Each side of the octagonal shape polystyrene block is loaded with 1 × 2 elements MIMO antenna array. The proposed 16-port MIMO antenna configuration with and without metamaterial decoupling structure is shown in Fig. 10. Each face contains two antenna elements placed at 0° and 180° angle (across-arrangement). The antenna elements placed across has a port-to-port distance of 36 mm. A copper sheet of thickness 0.5 mm and width 3.5 mm is used to connect the ground planes of the MIMO elements. All sixteen antenna elements have a common connected ground plane, which is very important in the practical implementation of MIMO antenna systems. A slight change in operating bandwidth and mutual coupling between array elements is observed with a common connected ground plane configuration. Whereas, side-by-side antennas, placed at the adjacent side of the block, have a port-to-port distance of 21.5 mm. The MIMO elements are arranged in a compact octagonal-shaped arrangement, which creates a strong mutual coupling between array placed in all configurations, i.e. antennas placed across at 180° angle (Ant. 1 and Ant. 2), side-by-side adjacent antenna at 45° (Ant. 1 and Ant. 3) and antenna elements in diagonal configuration (Ant. 1 and Ant. 4). Therefore, an effective decoupling structure is required to reduce mutual coupling in all configurations. Therefore, an H-shaped near-zero-index epsilon negative (NZI-ENG) metamaterial-decoupling structure is designed for non-planar array configuration.

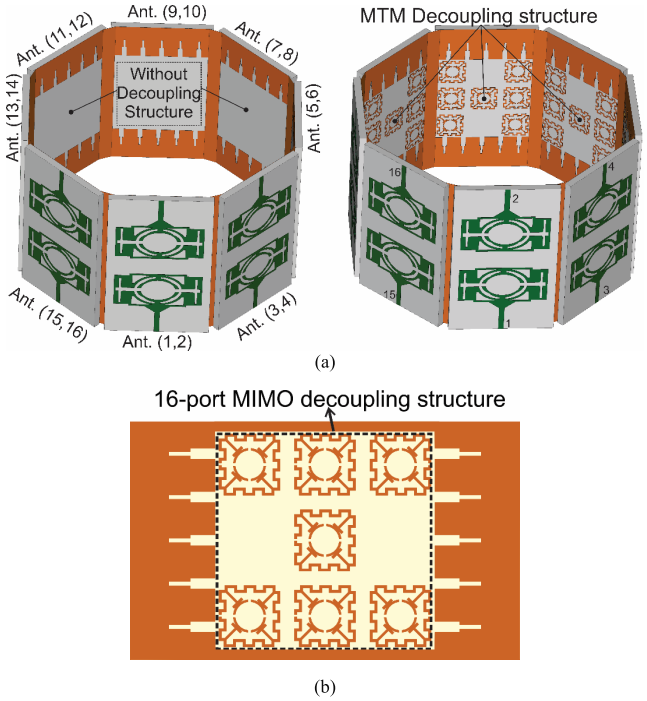

FIGURE 10. 16-port non-planar MIMO prototype. (a). MIMO antenna system with and without decoupling structure. (b). H-shape decoupling structure.

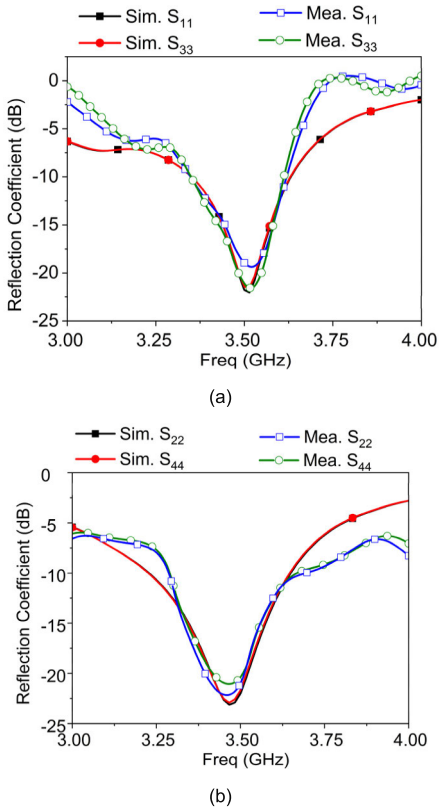

FIGURE 11. 16-port MIMO antenna system reflection coefficient. (a). Side-by-side elements. (b). Antenna elements placed across.

The physical phenomena of metamaterial-based decoupling metamaterial is analyzed by using the surface current distribution. The MTM elements placed behind the radiating patch have low surface current distribution. In contrast, high surface current distribution is observed on the MTM elements place at the radiator corners and middle of the two MIMO elements. Therefore, MTM elements with low surface current distribution have been removed from the metamaterial array. The modified H-shape decoupling structure provides better isolation, high surface current distribution and suppresses the unwanted strong induction currents, when antenna elements are arranged in 3D-arrangement (side-by-side elements at 45°, across elements at 180° and diagonally placed elements). Moreover, by using the modified H-shape decoupling structure simulation time and computational resources significantly reduced for the 16-port non-planar MIMO antenna configuration.

IV. RESULTS AND DISCUSSION

A 16-port no-planar MIMO antenna is proposed for 5G applications. A good impedance matching along with low mutual coupling between array elements is imperative for the 5G-MIMO antenna design. A 1 × 2 MIMO array prototype is placed on each face of the octagonal-shaped polystyrene block. The antenna elements are symmetric and identical in the 3D non-planar arrangement. Therefore, impedance matching for adjacent elements is only considered for the octagonal-shape arrangement. Fig. 11 shows the measured and simulated reflection coefficient of side-by-side and across elements. The MIMO antenna elements in both configurations (side-by-side and across) has a reflection coefficient less than −10 dB at 3.5 GHz frequency band.

The mutual coupling of 16-port MIMO antenna system with and without metamaterial decoupling structure is shown in Fig. 12. High mutual coupling is observed for side-by-side and across elements without the metamaterial decoupling structure, as shown in Fig. 12. Besides, high mutual coupling is also observed on the adjacent elements, and mutual coupling gradually decreases on the MIMO elements placed far way. The mutual coupling reduction between the array elements is achieved by using the NZI-ENG metamaterial decoupling structure. In non-planar 3D-MIMO configurations, mutual coupling between array elements never exceeds −28 dB with H-shape decoupling structure.

Simulated and measured isolation of the proposed MIMO antenna configuration is shown in Fig. 13. In both configurations (side-by-side and across), isolation better than 28 dB is realized for 3.5 GHz frequency band. A lossless polystyrene block was used in the simulator to create a non-planar MIMO assembly. Therefore, additional effect of polystyrene material on the mutual coupling and reflection coefficient is not evident in the simulated results. A slight variation in simulated and measured isolation is observed for the proposed MIMO configuration. These variations are due to the imperfections in the non-planar 3D assembly.

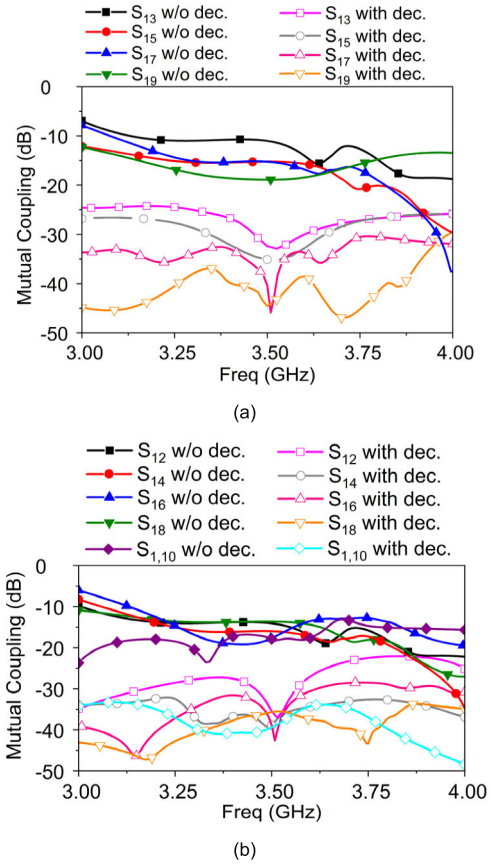

FIGURE 12. Mutual coupling of 16-port MIMO antenna with and without metamaterial decoupling structure. (a). Side-by-side elements. (b). Antenna elements place across at 180° angle.

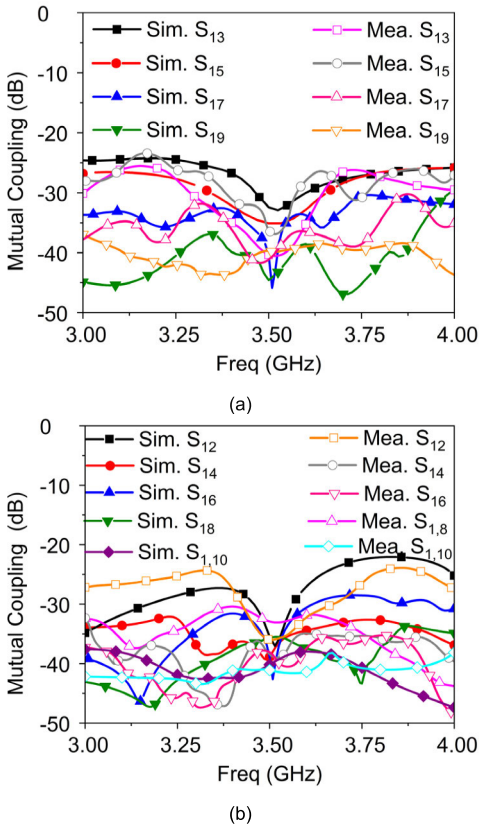

FIGURE 13. 16-port MIMO simulated and measured isolation performance. (a). Side-by-side elements. (b). Across elements (180°).

Overall, 3D polystyrene block is employed to hold the MIMO elements in non-planar configuration, without any contribution in isolation enhancement. The surface current distribution is employed to show the utility of the metamaterial-based decoupling structure. The surface current distribution on the 3D-MIMO antenna system is illustrated in Fig. 14. In the absence of MTM decoupling array, strong induction currents are present on the MIMO elements placed in the side-by-side and across configuration in non-planar configuration, as shown in Fig. 14 (a). The strong induced currents on the surrounding MIMO elements is suppressed by using the H-shape NZI-ENG metamaterial decoupling structure. A significant reduction in mutual coupling is found between MIMO elements by using the decoupling structure.

The surface current distribution in the presence of the MTM decoupling structure is shown in Fig. 14(b). ECC, TARC and CCL are used to evaluate the diversity performance of the 16-port MIMO antenna system. The value of TARC, ECC and CLL should be less than 0 dB, 0.5 and 0.5 bits/s/Hz, respectively, for an efficient non-planar MIMO antenna system [5].

The ECC, TARC and CCL values are extracted by using relations provided in [34]–[37]. Equation (11) is used to calculate the envelope correlation coefficient for antenna elements placed across and side-by-side configuration. The simulated and measured ECC is shown in Fig. 15(a). The CCL and TARC of the proposed MIMO antenna system in both configurations is calculated by using the equation (12) and (13). Simulated and measured CCL and TARC is portrayed in Fig. 15 (b) and (c). For the proposed 16-port non-planar MIMO configuration with a connected ground plane, ECC, CCL and TARC values are less than 0.1, 0.3 bits/s/Hz and −18 dB respectively for both antenna arrangements (side-by-side at 45° and antenna elements at 180° angle). Moreover, simulated and measured performance parameters values are within acceptable limits when decoupling is employed.

$$ECC = \frac{\left|\iint_{4\pi}\left[\vec{R}_i(\theta,\phi)\times\vec{R}_j(\theta,\phi)\right]d\Omega\right|^2}{\iint_{4\pi}\left|\vec{R}_i(\theta,\varphi)\right|^2 d\Omega \iint_{4\pi}\left|\vec{R}_j(\theta,\varphi)\right|^2 d\Omega} \tag{11}$$

$$CCL = -log_2 det\begin{bmatrix}\alpha_{11} & \alpha_{12}\\ \alpha_{21} & \alpha_{22}\end{bmatrix} \tag{12}$$

where i and j = 1, 2

$$\alpha_{ii} = 1 - \left|\sum_{n=1}^{n=2} S_{in}^* S_{ni}\right| \text{ and } \alpha_{ij} = -\left|\sum_{n=1}^{n=2} S_{in}^* S_{nj}\right| \tag{12a}$$

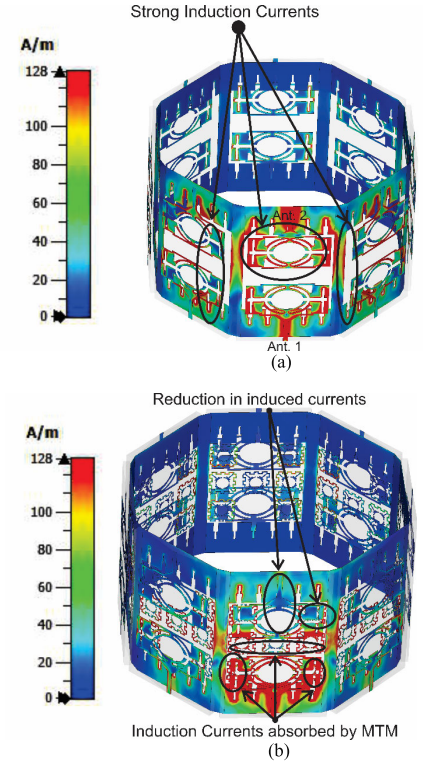

FIGURE 14. Surface current distribution on 16-port MIMO system. (a). Without MTM decoupling structure. (b). With MTM decoupling array.

$$TARC = \sqrt{\frac{\left|(S_{11} + S_{12}e^{j\theta})\right|^2 + \left|(S_{21} + S_{22}e^{j\theta})\right|^2}{2}} \tag{13}$$

The far-field radiation characteristics of fabricated MIMO antenna system are measured in Satimo measurement lab (UKM-star lab), by using the Agilent N5227A vector analyzer, Satimo passive measurement setup and SatEnv software [27], as shown in Fig. 17. Simulated and measured far-field radiation patterns of Ant. 1 and Ant. 2 in E and H-plane are shown in Fig. 16. During the ant.1 and ant.2 measurements, other MIMO elements are properly terminated with 50Ω load impedance. The radiation patterns in both planes are almost omnidirectional. However, a little difference in simulated and measured results is observed in both planes due to measurement setup constraints and imperfections in 3D non-planar array assembly. The 16-port MIMO antenna system far-field radiation characteristics (gain and efficiency) are plotted in Fig. 17. A measured gain of more than 6.5 Bi and an efficiency of more than 65% is realized for the non-planar array configuration.

The radiation efficiency and gain of the proposed MIMO antenna system are measured by employing the SATIMO near-field antenna measurement system. The 16-identical measurement probs in SATIMO measurement system are used to obtain the radiated near-field data by using the combination of the 360° horizontally rotating values of

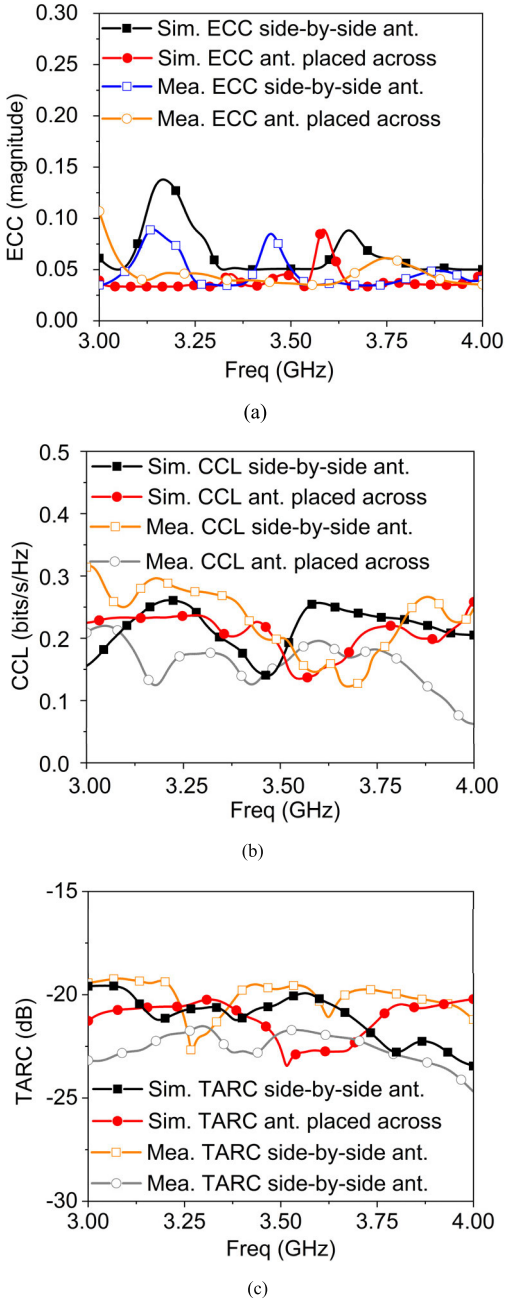

FIGURE 15. 16-port non-planar MIMO system performance parameters. (a). ECC. (b). CCL. (c). TARC.

proposed MIMO antenna and 3D scan values of the probes. The near-field data is then converted to far-field data through Fourier transformation (FT) to reveal the radiation patterns. Afterwards, efficiency and gain from the far-field data of the radiation pattern are calculated by using the SatEnv software.

The performance of the non-planar 3D-MIMO antenna system is compared with the recent state-of-the-art MIMO antenna systems in Table 3. It can be observed that high isolated, 3D-MIMO antenna system with NZI-ENG

TABLE 3. 16-port 3D non-planar MIMO antenna comparison with recent reported literature.

Ref. no	Geometry	Ports	Decoupling method	Gain (dBi)	Operating Band (GHz)	Isolation (dB)	ECC	CCL	TARC (dB)
[5]	Non-planar	4	FSS-Based decoupling structure	–	3–11	20	< 0.005	< 0.2	-8
[10]	Non-planar	2	Parasitic decoupling structure	–	3.1–10.6	20	< 0.1	< 0.7	- 4
[29]	Non-Planar	8	Distance based 3D elements configuration	6	3–11	20	< 0.5	–	–
[30]	Planar	8	Grounded slits based decoupling structure	–	2–11	15	< 0.2	–	-8
[31]	Planar	8	Orthogonal polarization with distance-based decoupling	3	2.5–2.7	12	< 0.12	–	–
[19]	Planar	10	Decoupling branches and neutralization lines	4.5	3.3–3.6, 4.8–5.0	12	< 0.15	< 0.08	–
[20]	Planar	12	Decoupling network (DN) technique	4	3.4–3.6	14	< 0.2	–	–
[32]	Planar	8	Slotting + Elements positioning	–	3.27–5.92	14.5	<0.1	–	–
[33]	Planar	8	Elements position + port Distance	5.6	3.2–6.1	18	<0.21	–	–
[17]	Non-planar	8	Parasitic decoupling Structure	7	3–11	20	< 0.0025	< 0.35	-11
This work	**Non-planar**	**16**	**ENG-NZI metamaterial decoupling Structure**	**6.5**	**3.35–3.65**	**28**	**< 0.1**	**< 0.3**	**-18**

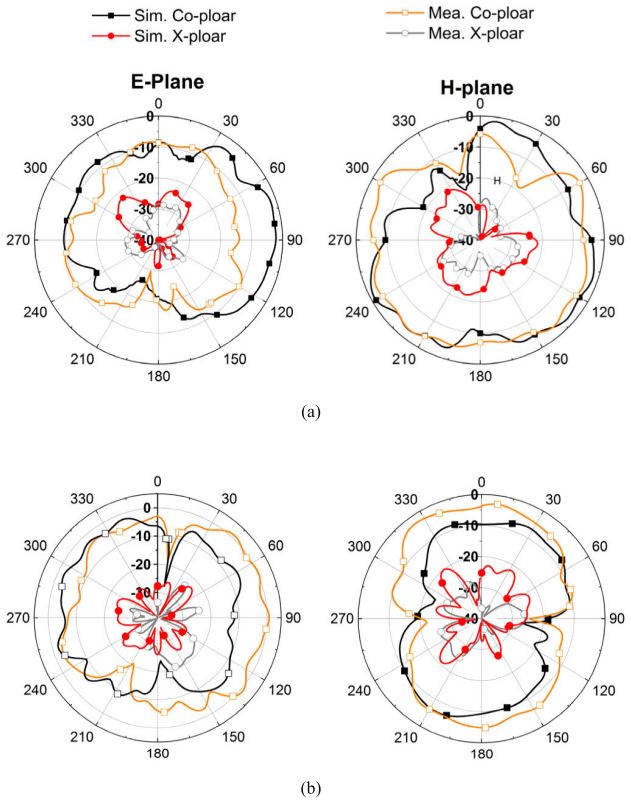

FIGURE 16. 16-port MIMO simulated and measured far-field radiation characteristics in E and H-plane. (a). Ant 1. (b). Ant 2.

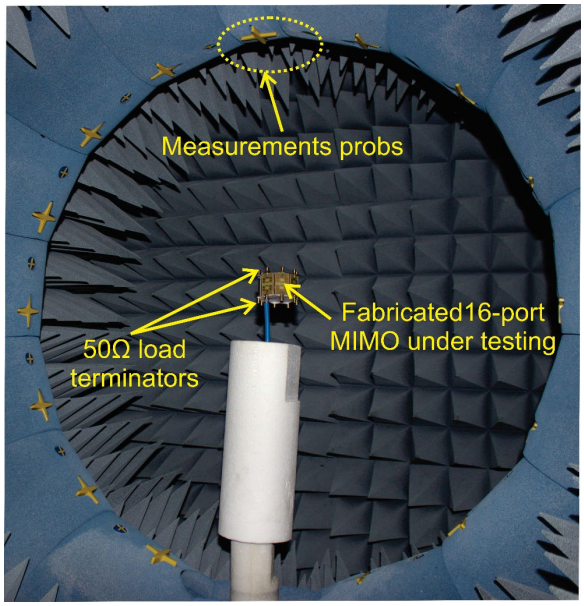

FIGURE 17. Fabricated MIMO prototype in the Satimo measurement lab (UKM-star lab).

metamaterial decoupling structure competes well with non-planar and planar MIMO antenna systems. In a compact non-planar arrangement, good impedance matching along with high isolation, good gain and radiation efficiency is very challenging to achieve in the rich scattering environment, without scarifying the MIMO performance parameters (CCL, TARC, ECC). Additionally, isolation of more than 28 dB, ECC < 0.1, CCL < 0.3, TARC < -18 dB, gain of 6.5 dBi and radiation efficiency greater than 65% realized for the all MIMO antenna elements, which is very competitive to planar and non-planar MIMO configurations.

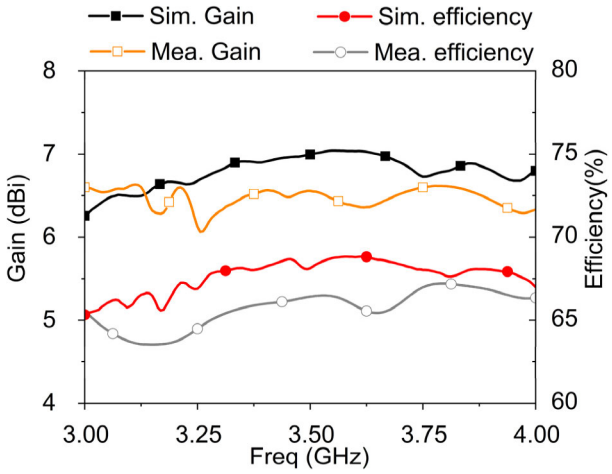

FIGURE 18. Simulated and measured gain and efficiency of 16-port MIMO antenna system.

V. CONCLUSION

In this paper, a 16-port non-planar MIMO antenna system with a metamaterial-based decoupling structure is proposed for 5th generation communication. The proposed 3D-MIMO configuration can be employed for the applications which require a miniaturized and non-planar arrangement. The slotted microstrip patch antenna ensures a proper impedance matching at 3.35 to 3.65 GHz frequency band. Moreover, near-zero-index epsilon-negative (NZI-ENG) metamaterial decoupling structure is employed to obtain an isolation of more than 28 dB in 3.35 to 3.65 GHz frequency band. Moreover, performance of the proposed MIMO antenna system is evaluated by ECC, TARC and CCL. A good agreement between simulated and measured results is achieved and proved that the proposed MIMO can be a potential candidate for 5G systems. The 16-port non-planar 5G-MIMO antenna system is very helpful for off device placement where best reception is obtained. Moreover, upcoming research will be foreseen to be concentrated on the implementation of the proposed MIMO antenna system in future wireless indoor localization technique with irregular scenario based on the performance analysis of the received signal strength.

REFERENCES

[1] H. Wang, R. Zhang, Y. Luo, and G. Yang, "Compact eight-element antenna array for triple-band MIMO operation in 5G mobile terminals," *IEEE Access*, vol. 8, pp. 19433–19449, 2020.
[2] Y. Li, C.-Y.-D. Sim, Y. Luo, and G. Yang, "High-isolation 3.5 GHz eight-antenna MIMO array using balanced open-slot antenna element for 5G smartphones," *IEEE Trans. Antennas Propag.*, vol. 67, no. 6, pp. 3820–3830, Jun. 2019.
[3] R. Li, Z. Mo, H. Sun, X. Sun, and G. Du, "A low-profile and high-isolated MIMO antenna for 5G mobile terminal," *Micromachines*, vol. 11, no. 4, p. 360, Mar. 2020.
[4] H. Al-Saif, M. Usman, M. T. Chughtai, and J. Nasir, "Compact ultra-wide band MIMO antenna system for lower 5G bands," *Wireless Commun. Mobile Comput.*, vol. 2018, pp. 1–6, Jun. 2018.
[5] M. Bilal, R. Saleem, H. H. Abbasi, M. F. Shafique, and A. K. Brown, "An FSS-based nonplanar quad-element UWB-MIMO antenna system," *IEEE Antennas Wireless Propag. Lett.*, vol. 16, pp. 987–990, Oct. 2017.
[6] T. Hassan, M. U. Khan, H. Attia, and M. S. Sharawi, "An FSS based correlation reduction technique for MIMO antennas," *IEEE Trans. Antennas Propag.*, vol. 66, no. 9, pp. 4900–4905, Sep. 2018.
[7] S. Zhang and G. F. Pedersen, "Mutual coupling reduction for UWB MIMO antennas with a wideband neutralization line," *IEEE Antennas Wireless Propag. Lett.*, vol. 15, pp. 166–169, May 2016.
[8] M. A. Ul Haq and S. Koziel, "Ground plane alterations for design of high-isolation compact wideband MIMO antenna," *IEEE Access*, vol. 6, pp. 48978–48983, 2018.
[9] F. Wang, Z. Duan, S. Li, Z.-L. Wang, and Y.-B. Gong, "Compact UWB MIMO Antenna with Metamaterial-Inspired Isolator," *Prog. Electromagn. Res. C*, vol. 84, pp. 61–74, 2018.
[10] S. I. Jafri, A. K. Brown, M. F. Shafique, and R. Saleem, "Compact reconfigurable multiple-input-multiple-output antenna for ultra wideband applications," *IET Microw., Antennas Propag.*, vol. 10, no. 4, pp. 413–419, Mar. 2016.
[11] S. R. Thummaluru and R. K. Chaudhary, "Mu-negative metamaterial filter-based isolation technique for MIMO antennas," *Electron. Lett.*, vol. 53, no. 10, pp. 644–646, May 2017.
[12] P. Garg and P. Jain, "Isolation improvement of MIMO antenna using a novel flower shaped metamaterial absorber at 5.5 GHz WiMAX band," *IEEE Trans. Circuits Syst. II, Exp. Briefs*, vol. 67, no. 4, pp. 675–679, Apr. 2020.
[13] S. Roy and U. Chakraborty, "Mutual coupling reduction in a multi-band MIMO antenna using meta-inspired decoupling network," *Wireless Pers. Commun.*, pp. 1–16, May 2020, doi: 10.1007/s11277-020-07526-5.
[14] B. C. Pan, W. X. Tang, M. Q. Qi, H. F. Ma, Z. Tao, and T. J. Cui, "Reduction of the spatially mutual coupling between dual-polarized patch antennas using coupled metamaterial slabs," *Sci. Rep.*, vol. 6, no. 1, p. 30288, Sep. 2016.
[15] Y. Xia, S. Luo, and Y. Li, "MIMO antenna array decoupling based on a metamaterial structure," in *Proc. IEEE Asia–Pacific Conf. Antennas Propag. (APCAP)*, Aug. 2018, pp. 383–384.
[16] J. Jiang, Y. Xia, and Y. Li, "High isolated X-band mimo array using novel wheel-like metamaterial decoupling structure," *Appl. Comput. Electromagn. Soc. J.*, vol. 34, no. 12, pp. 1829–1836, 2019.
[17] T. Shabbir, R. Saleem, S. S. Al-Bawri, M. F. Shafique, and M. T. Islam, "Eight-port metamaterial loaded UWB-MIMO antenna system for 3D system-in-package applications," *IEEE Access*, vol. 8, pp. 106982–106992, 2020.
[18] S. K. Palaniswamy, Y. P. Selvam, M. G. N. Alsath, M. Kanagasabai, S. Kingsly, and S. Subbaraj, "3-D eight-port ultrawideband antenna array for diversity applications," *IEEE Antennas Wireless Propag. Lett.*, vol. 16, pp. 569–572, Jul. 2017.
[19] W. Hu, X. Liu, S. Gao, L.-H. Wen, L. Qian, T. Feng, R. Xu, P. Fei, and Y. Liu, "Dual-band ten-element MIMO array based on dual-mode IFAs for 5G terminal applications," *IEEE Access*, vol. 7, pp. 178476–178485, 2019.
[20] M.-Y. Li, Y.-L. Ban, Z.-Q. Xu, J. Guo, and Z.-F. Yu, "Tri-polarized 12-antenna MIMO array for future 5G smartphone applications," *IEEE Access*, vol. 6, pp. 6160–6170, 2018.
[21] A. Ren, Y. Liu, and C.-Y.-D. Sim, "A compact building block with two shared-aperture antennas for eight-antenna MIMO array in metal-rimmed smartphone," *IEEE Trans. Antennas Propag.*, vol. 67, no. 10, pp. 6430–6438, Oct. 2019.
[22] M. Ullah, M. Islam, and M. Faruque, "A near-zero refractive index meta-surface structure for antenna performance improvement," *Materials*, vol. 6, no. 11, pp. 5058–5068, Nov. 2013.
[23] S. S. Islam, M. R. I. Faruque, and M. T. Islam, "A near zero refractive index metamaterial for electromagnetic invisibility cloaking operation," *Materials*, vol. 8, no. 8, pp. 4790–4804, 2013.
[24] S. S. Islam, M. R. I. Faruque, and M. T. Islam, "A new direct retrieval method of refractive index for the metamaterial," *Current Sci.*, vol. 109, no. 2, pp. 337–342, 2015.
[25] S. S. Al-Bawri, H. Hwang Goh, M. S. Islam, H. Y. Wong, M. F. Jamlos, A. Narbudowicz, M. Jusoh, T. Sabapathy, R. Khan, and M. T. Islam, "Compact ultra-wideband monopole antenna loaded with metamaterial," *Sensors*, vol. 20, no. 3, p. 796, Jan. 2020.
[26] A. B. Numan and M. S. Sharawi, "Extraction of material parameters for metamaterials using a full-wave simulator [education column]," *IEEE Antennas Propag. Mag.*, vol. 55, no. 5, pp. 202–211, Oct. 2013.
[27] A. Salleh, C. C. Yang, T. Alam, M. S. J. Singh, M. Samsuzzaman, and M. T. Islam, "Development of microwave brain stroke imaging system using multiple antipodal Vivaldi antennas based on raspberry pi technology," *J. Eng.*, vol. 32, no. 1, pp. 39–49, 2020.

[28] M. A. W. Nordin, M. T. Islam, and N. Misran, "Design of a compact ultra-wideband metamaterial antenna based on the modified split-ring resonator and capacitively loaded strips unit cell," *Prog. Electromagn. Res.*, vol. 136, pp. 157–173, 2013.
[29] M. S. Khan, F. Rigobello, B. Ijaz, E. Autizi, A. D. Capobianco, R. Shubair, and S. A. Khan, "Compact 3-D eight elements UWB-MIMO array," *Microw. Opt. Technol. Lett.*, vol. 60, no. 8, pp. 1967–1971, Aug. 2018.
[30] R. Mathur and S. Dwari, "8-port multibeam planar UWB-MIMO antenna with pattern and polarisation diversity," *IET Microw., Antennas Propag.*, vol. 13, no. 13, pp. 2297–2302, Oct. 2019.
[31] M.-Y. Li, Z.-Q. Xu, Y.-L. Ban, C.-Y.-D. Sim, and Z.-F. Yu, "Eight-port orthogonally dual-polarised MIMO antennas using loop structures for 5G smartphone," *IET Microw., Antennas Propag.*, vol. 11, no. 12, pp. 1810–1816, Sep. 2017.
[32] H.-D. Chen, Y.-C. Tsai, C.-Y.-D. Sim, and C. Kuo, "Broadband eight-antenna array design for sub-6 GHz 5G NR bands metal-frame smartphone applications," *IEEE Antennas Wireless Propag. Lett.*, vol. 19, no. 7, pp. 1078–1082, Jul. 2020.
[33] A. Singh and C. E. Saavedra, "Wide-bandwidth inverted-F stub fed hybrid loop antenna for 5G sub-6 GHz massive MIMO enabled handsets," *IET Microw., Antennas Propag.*, vol. 14, no. 7, pp. 677–683, Jun. 2020.
[34] Z. Wang, C. Li, Q. Wu, and Y. Yin, "A metasurface-based low-profile array decoupling technology to enhance isolation in MIMO antenna systems," *IEEE Access*, vol. 8, pp. 125565–125575, 2020.
[35] U. Ullah, M. Al-Hasan, S. Koziel, and I. B. Mabrouk, "Circular polarization diversity implementation for correlation reduction in wideband low-cost multiple-input-multiple-output antenna," *IEEE Access*, vol. 8, pp. 95585–95593, 2020.
[36] N. Hussain, M.-J. Jeong, A. Abbas, and N. Kim, "Metasurface-based single-layer wideband circularly polarized MIMO antenna for 5G millimeter-wave systems," *IEEE Access*, vol. 8, pp. 130293–130304, 2020.
[37] M. S. Sharawi, "Current misuses and future prospects for printed multiple-input, multiple-output antenna systems [wireless corner]," *IEEE Antennas Propag. Mag.*, vol. 59, no. 2, pp. 162–170, Apr. 2017.
[38] J. Wen, J. Weng, C. Tong, C. Ren, and Z. Zhou, "Sparse signal recovery with minimization of 1-Norm minus 2-Norm," *IEEE Trans. Veh. Technol.*, vol. 68, no. 7, pp. 6847–6854, Jul. 2019.

TAYYAB SHABBIR received the B.S. degree in electrical engineering from the COMSATS Institute of Information Technology (CIIT), Islamabad, Pakistan, in 2011, and the master's degree in telecommunication engineering and the Ph.D. degree in antennas and electromagnetics from the University of Engineering and Technology (UET) at Taxila, Taxila, Pakistan, in 2014 and 2019, respectively. He is currently working as a Postdoctoral Researcher with the Department of Electrical, Electronic and Systems Engineering, Universiti Kebangsaan Malaysia (UKM), Malaysia. He has published articles in many reputable scientific journals and conferences. His current research interests include UWB-MIMO systems, 3D non-planar MIMO systems, metamaterials, high gain portable devices, and frequency selective surfaces and reflectarrays. He was a recipient of a fully-funded scholarship for the master's and Ph.D. degrees.

MOHAMMAD TARIQUL ISLAM (Senior Member, IEEE) is currently a Professor with the Department of Electrical, Electronic and Systems Engineering, Universiti Kebangsaan Malaysia (UKM), and a Visiting Professor with the Kyushu Institute of Technology, Japan. He has supervised about 30 Ph.D. degree theses, 20 M.Sc. degree theses, and has mentored more than ten postdoctoral and visiting scholars. He has authored and coauthored over 500 research journal articles, nearly 175 conference articles, and a few book chapters on various topics related to antennas, metamaterials, and microwave imaging with 22 inventory patents filed. Thus far, his publications have been cited 6185 times, and his H-index is 38 (source: Scopus). His Google scholar citation is 9000 and H-index is 45. He was a recipient of more than 40 research grants from the Malaysian Ministry of Science, Technology and Innovation, Ministry of Education, the UKM research grant, and international research grants from Japan and Saudi Arabia. His research interests include communication antenna design, metamaterial, satellite antennas, and microwave imaging. He has been serving as an Executive Committee Member of the IEEE AP/MTT/EMC Malaysia Chapter, since 2018, a Chartered Professional Engineer (C.Eng.), a member of IET, U.K., and a Senior Member of IEICE, Japan. He received several international gold medal awards, the Best Invention in Telecommunication Award for his research and innovation, and the Best Researcher Awards from the UKM from 2010 to 2011. He was a recipient of the IEEE AP/MTT/EMC Malaysia Chapter Excellent Award from 2018 to 2019. He also won the Best Innovation Award in 2011 and the Best Research Group in ICT Niche from the UKM in 2014. He was a recipient of the Publication Award from the Malaysian Space Agency, in 2009, 2010, 2013, and 2014, and the Best Paper Presentation Award from the International Symposium on Antennas and Propagation (ISAP 2012), Nagoya, Japan, in 2012, and IconSpace in 2015. He was an Associate Editor of *IET Electronics Letter*. He also serves as a Guest Editor for *Sensors* journal and an Associate Editor for IEEE Access.

SAMIR SALEM AL-BAWRI (Member, IEEE) received the M.Sc. degree in wireless communication engineering from Yarmouk University, Jordan, in 2009, and the Ph.D. degree in communication engineering from Universiti Malaysia Perlis (UniMAP), Malaysia, in 2018. He has served as a Lecturer with the Faculty of Engineering and Petroleum, Hadhramout University (HU), Yemen, from December 2009 to August 2014. He served as a Graduate Research Assistance with the UniMAP from 2015 to 2018. He has served as a Postdoctoral Researcher Fellow of Multimedia University (MMU), Cyberjaya, Malaysia, for one year. He is currently affiliated with the Center for Space Science, Institut Perubahan Iklim, Universiti Kebangsaan Malaysia (UKM). He has authored or coauthored over 15 ISI and Scopus published journals, and 19 conference proceedings. He is currently working toward the first patent. His research interests include the design and evaluation of multi-element antennas, metamaterials, electromagnetic radiation analysis, localization estimation techniques, and wireless propagation. He currently serves as the Editor Manager of the *International Journal of Multidisciplinary Sciences and Advanced Technology (IJMSAT).* He was a recipient of the Gold Medal Award from the Breakthrough Invention, Innovation, and Design Exhibition Biide–UiTM in 2019.

RABAH W. ALDHAHERI (Member, IEEE) received the Ph.D. degree in electrical and computer engineering from Michigan State University, in 1988. He has served as the Head of the Department of Electrical and Computer Engineering, KAU, from May 2005 to May 2011. He has held visiting research scholar positions at Michigan State University from 1994 to 1995 and the Queensland University of Technology (QUT), Brisbane, Australia, in 2000. He is currently serving as the Founder and the Director of the Microelectronics and RF Circuits Laboratory the FSS and Metamaterial Research Laboratory, and the Head of the Communication Systems and Networks Research Group. He is currently a Full Professor with the Department of Electrical and Computer Engineering, King Abdulaziz University (KAU), Jeddah, Saudi Arabia. His research interests include digital signal processing with applications to filter design and biometric recognition, microelectronics devices, and wireless communications, particularly, antennas design for UWB communication, RFID readers, and frequency selective surfaces (FSS). He served as a Reviewer for many national and international journals in the areas of system modeling, DSP, digital communication, and antennas design. He is an Associate Editor of the *Journal of Applied Sciences*.

KHALID HAMED ALHARBI received the Ph.D. degree in electrical engineering from the University of Glasgow, in 2016. He is currently an Assistant Professor with the Department of Electrical and Computer Engineering, King Abdulaziz University. His research interests include micro/nano-fabrication technologies, millimeter-wave and THz antennas, and RTD-based devices.

ABDULAH JEZA ALJOHANI (Member, IEEE) received the B.Sc.Eng. degree in electronics and communication engineering from King Abdulaziz University, Jeddah, Saudi Arabia, in 2006, and the M.Sc. (Hons.) and Ph.D. degrees in wireless communication from the University of Southampton, Southampton, U.K., in 2010. He is currently an Assistance Professor with the Department of Electrical and Computer Engineering, King Abdulaziz University. His research interests include joint source/channel coding, distributed source coding, free-space optical communication, channel coding, cooperative communications, and MIMO systems.

RASHID SALEEM received the B.S. degree in electronics engineering from the Ghulam Ishaq Khan Institute of Engineering Sciences and Technology, Pakistan, in 1999, the M.S. degree from the Center for Advanced Studies in Engineering, University of Engineering and Technology (UET) at Taxila, Taxila, Pakistan, in 2006, and the Ph.D. degree from The University of Manchester, U.K., in 2011. He pursued a career in the telecommunication industry for several years while continuing education. In the Ph.D. degree, he worked with the Microwave and Communication Systems Research Group, under the supervision of Prof. A. K. Brown, and the Head of the School of Electrical and Electronics Engineering, The University of Manchester. He worked on antennas, channel modeling, and interference aspects of ultra-wideband systems during the Ph.D. degree and was also a member of a team designing and testing arrays for the Square Kilometer Array Project. He is currently working as a Tenured Associate Professor with the UET at Taxila, where he is supervising several master's degree students and the Head of the Microwaves, Antennas, and Propagation (MAP) Research Group. His research interests include antennas, angle-of-arrival-based channel modeling, microwave periodic structures, and metamaterials.